DINAME 2023 - Proceedings of the XIX International Symposium on Dynamic Problems of Mechanics,
A.S. De Paula, A.T. Fabro and M.R. Machado (Editors), ABCM.
Pirenópolis, Go, Brazil, February 26th to March 3rd, 2023

Numerical investigation of a zig-zag beam-type quasi-periodic structure with multiple defects

Vinícius Mauro de Souza Santos[1], **and Thiago de Paula Sales**[1]

[1] Aeronautics Institute of Technology, Pç. Mal. Eduardo Gomes, 50 – Vila das Acácias, São José dos Campos, SP, Brazil

Abstract: Periodic structures have been intensively studied lately, as they possess unusual behavior related to wave propagation that can be deeply explored in various academic and industrial applications. In this work, we investigate the dynamic behavior of a zig-zag beam-type quasi-periodic lattice, embedded with multiple geometrical "defects", which break perfect periodicity of the mechanical system. The quasi-periodic structure is modeled using the wave-based finite element method (WFEM), duly modified to allow for distinct unit cells along the lattice. Results obtained from simulations show that the presence of two defective unit cells enables the formation of additional regions in which mechanical energy gets confined – which can be significant for energy harvesting applications, for example.

Keywords: quasi-periodicity, localized modes, multiple defects, WFEM

INTRODUCTION

The study of periodic structures has attracted the attention of the scientific community over the years as they enable the engineering of unusual properties that are not encountered in traditional systems, e.g., the appearance of bandgaps (Mizukami et al., 2021), waveguiding (Pal and Ruzzene, 2017), structure-borne sound and confinement (Assouar et al., 2012), and mode localization phenomenon (Bendiksen, 2000). Of course, these phenomena have been leveraged in various real engineering applications, most of them related to the mitigation of noise and vibrations in mechanical systems, which can be of great value for industrial applications.

The phenomenon of mode localization usually appears in quasi-periodic structures, which are made by introducing one or more defects in a periodic lattice. A defect corresponds, basically, to a break in periodicity, which can be realized by means of geometrical or material changes, being these intentional or not. Cunha (2017), for example, has considered a quasi-periodic beam-type structure, with ten unit cells. In a quasi-periodic mechanical system, the energy due to an excitation can become localized at the defect zone (defect mode) for certain frequencies, being not widespread throughout its whole domain. In this context, the use of localized defects in periodic systems can inhibit the propagation of motion and energy out of the location where a defect is. More recently, phononic crystals with defects were investigated by Jo et al. (2020), whom exploited the mode localization phenomenon aiming for energy harvesting, employing piezoelectric materials.

As stated by Hodges (1982), the localization phenomenon was first studied by physicists in the fifties (Anderson, 1958). In addition, the work of Hodges (1982), which was concerned with coupled pendula and a bending beam, is supposed to be the first that investigated the localization phenomenon in quasi-periodic structures of interest to structural dynamicists. Luongo (1992) studied continuous one-dimensional systems with a single localized defect, and showed the occurrence of modes at the imperfection region for some types of boundary conditions. The analysis of defects diffused along the beam was also carried out by Luongo (1992). Zhu and Semperlotti (2013) explored quasi-periodic structures with tunable defects, which can be used for passive vibration control and energy harvesting.

Despite the abundant literature that investigates the influence of an isolated defect in quasi-periodic structures, some of them briefly discussed above, the dynamic behavior of systems that possess a couple of imperfections seems to require investigation. Hence, in this work, one aims to characterize how the relative position of defects in a quasi-periodic structure affects its behavior. To perform analyzes, the wave-based finite element method (WFEM) (Hoang et al., 2018) is considered, with it being duly modified to model structures composed of more than one waveguide (WG) (Santos, 2022). In this setting, the behavior of the system which is considered can be represented by relying on Bloch-Floquet wavemodes related to defective and non-defective unit cells, enabling relatively low computational cost. The underlying periodic structure which is investigated corresponds to a zig-zag beam, cf. Fig. 1, largely used in applications which demand relatively low resonance frequency and have limited space availability. Transmissibilities and harmonic deformed shapes are obtained to assess the system behavior, and investigate if and how the relative position of defects influence its dynamics.

MODELING

The presentation given here for the WFEM is essentially a summary of the works of Hoang et al. (2018), and Mencik and Duhamel (2015). The modeling description of the zig-zag beam type structure begins with fundamental developments,

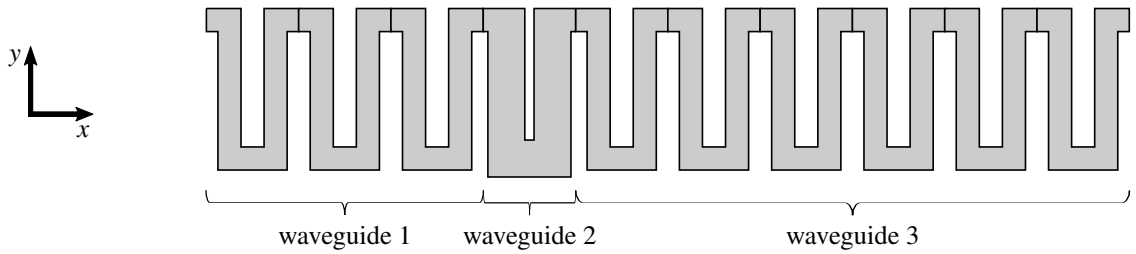

Figure 1 – Zig-zag beam-type quasi-periodic structure.

followed by wave modes computation using the Bloch-Floquet theorem. The system forced response is obtained in the sequence by relying on the basis formed by the wave modes.

Consider a periodic structure formed by N unit cells, as shown in Fig. 2. For a unit cell which is modeled by the traditional FEM, the degrees of freedom (DOFs) and loads' vectors can be partitioned according to their location being left, right or internal. These partitions are denoted, respectively, by $\mathbf{q}_j$ and $\mathbf{F}_j$, for $j \in \{L,R,I\}$.

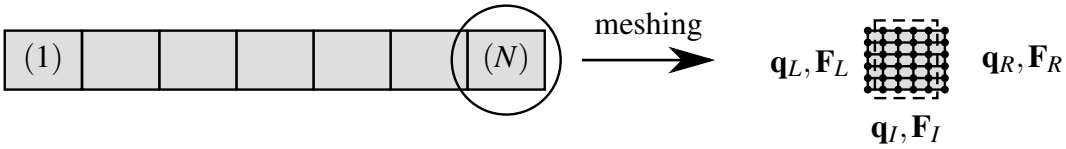

Figure 2 – Periodic structure containing N unit cells and the mesh of one of its cells.

The equations of motion for the unit cell highlighted in Fig. 2 can be expressed as $\mathbf{M}\ddot{\mathbf{q}} + \mathbf{C}\dot{\mathbf{q}} + \mathbf{K}\mathbf{q} = \mathbf{f}$, where $\mathbf{M}$, $\mathbf{C}$ and $\mathbf{K}$ are the matrices of mass, damping and stiffness, respectively, $\mathbf{f}$ is the load's vector, $\mathbf{q}$, $\dot{\mathbf{q}}$ and $\ddot{\mathbf{q}}$ are vectors of generalized displacements, velocities and accelerations.

In the frequency domain, we can write $\mathbf{D}\mathbf{q} = \mathbf{F}$, where $\mathbf{D} = -\omega^2\mathbf{M} + \mathrm{i}\,\omega\mathbf{C} + \mathbf{K}$ is the dynamic stiffness matrix (DSM). Another possible version of $\mathbf{D}$, which also considers damping, is written as $\mathbf{D} = -\omega^2\mathbf{M} + (1+\mathrm{i}\eta)\,\mathbf{K}$, where η is the structural damping coefficient (Renno and Mace, 2010). Segregating the DOFs and nodal loads according to the previously mentioned partition, we can write:

$$\begin{bmatrix} \tilde{\mathbf{D}}_{LL} & \tilde{\mathbf{D}}_{LR} & \tilde{\mathbf{D}}_{LI} \\ \tilde{\mathbf{D}}_{RL} & \tilde{\mathbf{D}}_{RR} & \tilde{\mathbf{D}}_{RI} \\ \tilde{\mathbf{D}}_{IL} & \tilde{\mathbf{D}}_{IR} & \tilde{\mathbf{D}}_{II} \end{bmatrix} \begin{Bmatrix} \mathbf{q}_L \\ \mathbf{q}_R \\ \mathbf{q}_I \end{Bmatrix} = \begin{Bmatrix} \mathbf{F}_L \\ \mathbf{F}_R \\ \mathbf{F}_I \end{Bmatrix}, \tag{1}$$

which provide an expression for the internal DOFs, i.e.,

$$\mathbf{q}_I = \tilde{\mathbf{D}}_{II}^{-1}(-\tilde{\mathbf{D}}_{IL}\mathbf{q}_L - \tilde{\mathbf{D}}_{IR}\mathbf{q}_R + \mathbf{F}_I). \tag{2}$$

Condensing the internal DOFs we are able to write

$$\begin{bmatrix} \mathbf{D}_{LI}\mathbf{F}_I \\ \mathbf{D}_{RI}\mathbf{F}_I \end{bmatrix} + \begin{bmatrix} \mathbf{D}_{LL} & \mathbf{D}_{LR} \\ \mathbf{D}_{RL} & \mathbf{D}_{RR} \end{bmatrix} \begin{Bmatrix} \mathbf{q}_L \\ \mathbf{q}_R \end{Bmatrix} = \begin{Bmatrix} \mathbf{F}_L \\ \mathbf{F}_R \end{Bmatrix}, \tag{3}$$

where:

$$\begin{aligned} &\mathbf{D}_{LL} = \tilde{\mathbf{D}}_{LL} - \tilde{\mathbf{D}}_{LI}\tilde{\mathbf{D}}_{II}^{-1}\tilde{\mathbf{D}}_{IL}, && \mathbf{D}_{LR} = \tilde{\mathbf{D}}_{LR} - \tilde{\mathbf{D}}_{LI}\tilde{\mathbf{D}}_{II}^{-1}\tilde{\mathbf{D}}_{IR}, && \mathbf{D}_{LI} = \tilde{\mathbf{D}}_{LI}\tilde{\mathbf{D}}_{II}^{-1}, \\ &\mathbf{D}_{RL} = \tilde{\mathbf{D}}_{RL} - \tilde{\mathbf{D}}_{RI}\tilde{\mathbf{D}}_{II}^{-1}\tilde{\mathbf{D}}_{IL}, && \mathbf{D}_{RR} = \tilde{\mathbf{D}}_{RR} - \tilde{\mathbf{D}}_{RI}\tilde{\mathbf{D}}_{II}^{-1}\tilde{\mathbf{D}}_{IR}, && \mathbf{D}_{RI} = \tilde{\mathbf{D}}_{RI}\tilde{\mathbf{D}}_{II}^{-1}. \end{aligned} \tag{4}$$

From Eq. (3), keeping in mind that it holds for the unit cell (n), one can get a relationship between the left and right quantities plus a term related to internal loads, as follows:

$$\begin{Bmatrix} \mathbf{q}_R^{(n)} \\ \mathbf{F}_R^{(n)} \end{Bmatrix} = \begin{bmatrix} -\mathbf{D}_{LR}^{-1}\mathbf{D}_{LL} & -\mathbf{D}_{LR}^{-1} \\ \mathbf{D}_{RL} - \mathbf{D}_{RR}\mathbf{D}_{LR}^{-1}\mathbf{D}_{LL} & -\mathbf{D}_{RR}\mathbf{D}_{LR}^{-1} \end{bmatrix} \begin{Bmatrix} \mathbf{q}_L^{(n)} \\ -\mathbf{F}_L^{(n)} \end{Bmatrix} + \begin{bmatrix} -\mathbf{D}_{LR}^{-1}\mathbf{D}_{LI} \\ \mathbf{D}_{RI} - \mathbf{D}_{RR}\mathbf{D}_{LR}^{-1}\mathbf{D}_{LI} \end{bmatrix} \mathbf{F}_I^{(n)}. \tag{5}$$

By enforcing DOFs' compatibility and load equilibrium between adjacent unit cells, namely (n) and $(n+1)$, i.e., $\mathbf{q}_R^{(n)} = \mathbf{q}_L^{(n+1)}$ and $\mathbf{F}_R^{(n)} = -\mathbf{F}_L^{(n+1)} + \mathbf{F}_B^{(n)}$, being $\mathbf{F}_B^{(n)}$ an external load applied to the right interface of cell (n), we obtain:

$$\mathbf{u}_L^{(n+1)} = \mathbf{S}\mathbf{u}_L^{(n)} + \mathbf{b}^{(n)}, \tag{6}$$

with:

$$\mathbf{u}_L^{(n)} = \begin{Bmatrix} \mathbf{q}_L^{(n)} \\ -\mathbf{F}_L^{(n)} \end{Bmatrix}, \qquad \mathbf{S} = \begin{bmatrix} -\mathbf{D}_{LR}^{-1}\mathbf{D}_{LL} & -\mathbf{D}_{LR}^{-1} \\ \mathbf{D}_{RL} - \mathbf{D}_{RR}\mathbf{D}_{LR}^{-1}\mathbf{D}_{LL} & -\mathbf{D}_{RR}\mathbf{D}_{LR}^{-1} \end{bmatrix}, \qquad \mathbf{b}^{(n)} = \begin{Bmatrix} \mathbf{D}_{qI}\mathbf{F}_I^{(n)} \\ \mathbf{D}_{fI}\mathbf{F}_I^{(n)} - \mathbf{F}_B^{(n)} \end{Bmatrix}, \tag{7}$$

being $\mathbf{D}_{qI} = -\mathbf{D}_{LR}^{-1}\mathbf{D}_{LI}$ and $\mathbf{D}_{fI} = \mathbf{D}_{RI} - \mathbf{D}_{RR}\mathbf{D}_{LR}^{-1}\mathbf{D}_{LI}$. Moreover, $\mathbf{u}$ is known as the state vector, and $\mathbf{S}$ is recognized as the unit cell transfer matrix.

Based on the recurrence relation embedded in Eq. (6), it is possible to arrive at the following relationships:

$$\mathbf{u}_L^{(n+1)} = \mathbf{S}^n\mathbf{u}_L^{(1)} + \textstyle\sum_{k=1}^{n} \mathbf{S}^{n-k}\mathbf{b}^{(k)}, \tag{8}$$

$$\mathbf{u}_L^{(N+1)} = \mathbf{S}^{N+1-n}\mathbf{u}_L^{(n)} + \textstyle\sum_{k=n}^{N} \mathbf{S}^{N-k}\mathbf{b}^{(k)}, \tag{9}$$

which will support mathematical developments afterwards.

By invoking periodic boundary conditions through the Bloch-Floquet theorem, in other words $\mathbf{u}_L^{(n+1)} = e^{-\mathrm{i}k_j\Delta}\mathbf{u}_L^{(n)} = \mu_j\mathbf{u}_L^{(n)}$ (Brillouin, 1955), being Δ the length of the unit cell along the propagation direction and μ_j the propagation constant, and by assuming no external loads ($\mathbf{b}^{(n)} = \mathbf{0}$), from Eq. (6) we can obtain a standard eigenvalue problem, $\left(\mathbf{S} - \mu_j\mathbf{I}\right)\boldsymbol{\phi}_j = \mathbf{0}$. Its solution provides the eigenpairs μ_j and $\boldsymbol{\phi}_j$ ($j = 1, ..., 2n_b$), being n_b the number of DOFs pertaining to the left interface of the unit cell. Wavenumbers can be obtained using $k_j = (\ln\mu_j)/(-\mathrm{i}\Delta)$. Purely real and purely imaginary wavenumbers are related to propagating and evanescent waves, respectively, whereas a complex wavenumber characterizes an oscillating decaying wave (Mace et al., 2005).

The solution of the previously mentioned eigenproblem is not straightforward, nevertheless, because $\boldsymbol{\phi}_j$ comprises both displacements and loads, whose values can be largely disparate (Mencik, 2014; Waki et al., 2009b). As an alternative, we can consider (Mencik and Duhamel, 2015; Zhong and Williams, 1995):

$$\left[\left(\mathbf{N}\mathbf{J}\mathbf{L}^{\mathrm{T}} + \mathbf{L}\mathbf{J}\mathbf{N}^{\mathrm{T}}\right) - \lambda_j\mathbf{L}\mathbf{J}\mathbf{L}^{\mathrm{T}}\right]\mathbf{z}_j = \mathbf{0}, \tag{10}$$

being:

$$\mathbf{L} = \begin{bmatrix} \mathbf{0} & \mathbf{I} \\ \mathbf{D}_{LR} & \mathbf{0} \end{bmatrix}, \qquad \mathbf{N} = \begin{bmatrix} \mathbf{D}_{RL} & \mathbf{0} \\ -\left(\mathbf{D}_{LL} + \mathbf{D}_{RR}\right) & -\mathbf{I} \end{bmatrix}, \qquad \mathbf{J} = \begin{bmatrix} \mathbf{0} & \mathbf{I} \\ -\mathbf{I} & \mathbf{0} \end{bmatrix}; \tag{11}$$

λ_j and $\mathbf{z}_j$ correspond to the eigenvalues and eigenvectors of the alternative, well-conditioned eigenproblem. It can be shown that $\lambda_j = \mu_j + 1/\mu_j$, such that $\mu_j = \frac{1}{2}\left(\lambda_j \pm \sqrt{\lambda_j^2 - 4}\right)$. Prof of this can be found elsewhere (Mencik and Ichchou, 2005). As for the eigenvectors of the original problem, they can be retrieved by:

$$\boldsymbol{\phi}_j = \begin{bmatrix} \mathbf{I} & \mathbf{0} \\ \mathbf{D}_{RR} & \mathbf{I} \end{bmatrix}\mathbf{w}_j, \qquad \text{with} \qquad \mathbf{w}_j = \mathbf{J}\left(\mathbf{L}^{\mathrm{T}} - \tfrac{1}{\mu_j}\mathbf{N}^{\mathrm{T}}\right)\mathbf{z}_j. \tag{12}$$

Eigenvalues and associated eigenvectors can be separated into those related to positive, $(\mu_j, \boldsymbol{\phi}_j)$, and negative-going waves, $(\mu_j^*, \boldsymbol{\phi}_j^*)$ ($j = 1, ..., n_b$). If $|\mu_j| < 1$, it is related to a wave which propagates in the positive direction; otherwise, if $|\mu_j| > 1$, the corresponding wave propagates in the negative direction. If $|\mu_j| = 1$, we can exploit the power flow of the wave mode (Duhamel et al., 2006; Waki et al., 2009a).

After eigensolutions have been distinguished accordingly, they can be grouped into matrices as follows:

$$\boldsymbol{\mu} = \mathrm{diag}\left(\mu_1, \ldots, \mu_{n_b}\right), \qquad \boldsymbol{\Phi} = \begin{bmatrix} \boldsymbol{\phi}_1 & \ldots & \boldsymbol{\phi}_{n_b} \end{bmatrix} = \begin{bmatrix} \boldsymbol{\Phi}_q \\ \boldsymbol{\Phi}_F \end{bmatrix}, \tag{13}$$

$$\boldsymbol{\mu}^* = \mathrm{diag}\left(\mu_1^*, \ldots, \mu_{n_b}^*\right), \qquad \boldsymbol{\Phi}^* = \begin{bmatrix} \boldsymbol{\phi}_1^* & \ldots & \boldsymbol{\phi}_{n_b}^* \end{bmatrix} = \begin{bmatrix} \boldsymbol{\Phi}_q^* \\ \boldsymbol{\Phi}_F^* \end{bmatrix}, \tag{14}$$

where subscripts q and F identify partitions of the eigenvectors which are related to DOFs and loads.

Using the wave modes, we can write the state vector and external loads of the unit cell (n) as a linear combination, i.e.,

$$\mathbf{u}_L^{(n)} = \boldsymbol{\Phi}\mathbf{Q}^{(n)} + \boldsymbol{\Phi}^*\mathbf{Q}^{*(n)}, \tag{15}$$

$$\mathbf{b}^{(n)} = \boldsymbol{\Phi}\mathbf{Q}_B^{(n)} + \boldsymbol{\Phi}^*\mathbf{Q}_B^{*(n)}, \tag{16}$$

where $\mathbf{Q}^{(n)}$, $\mathbf{Q}^{*(n)}$, $\mathbf{Q}_B^{(n)}$ and $\mathbf{Q}_B^{*(n)}$ are amplitude vectors. After some manipulations of Eqs. (8) and (9), we get:

$$\mathbf{Q}^{(n)} = \boldsymbol{\mu}^{n-1}\mathbf{Q}^{(1)} + \textstyle\sum_{k=1}^{n-1} \boldsymbol{\mu}^{n-k-1}\mathbf{Q}_B^{(k)}, \tag{17}$$

$$\mathbf{Q}^{*(n)} = \boldsymbol{\mu}^{N+1-n}\mathbf{Q}^{*(N+1)} - \textstyle\sum_{k=n}^{N} \boldsymbol{\mu}^{k-n+1}\mathbf{Q}_B^{*(k)}, \tag{18}$$

being $\mathbf{Q}_B^{(k)}$ and $\mathbf{Q}_B^{*(k)}$ obtained manipulating Eq. (16), i.e.,

$$\mathbf{Q}_B^{(k)} = \left(\boldsymbol{\mu}\boldsymbol{\Phi}_q^{*\mathrm{T}}\mathbf{D}_{LI} + \boldsymbol{\Phi}_q^{*\mathrm{T}}\mathbf{D}_{RI}\right)\mathbf{F}_I^{(k)} - \boldsymbol{\Phi}_q^{*\mathrm{T}}\mathbf{F}_B^{(k)}, \tag{19}$$

$$\mathbf{Q}_B^{*(k)} = -\left(\boldsymbol{\mu}^*\boldsymbol{\Phi}_q^{\mathrm{T}}\mathbf{D}_{LI} + \boldsymbol{\Phi}_q^{\mathrm{T}}\mathbf{D}_{RI}\right)\mathbf{F}_I^{(k)} + \boldsymbol{\Phi}_q^{\mathrm{T}}\mathbf{F}_B^{(k)}. \tag{20}$$

Recalling that the state vector $\mathbf{u}_L^{(n)}$ contains information related to DOFs and loads, as well as the partition introduced in Eq. (13), we can obtain:

$$\mathbf{q}_L^{(n)} = \boldsymbol{\Phi}_q\boldsymbol{\mu}^{n-1}\mathbf{Q} + \boldsymbol{\Phi}_q^*\boldsymbol{\mu}^{N+1-n}\mathbf{Q}^* + \boldsymbol{\Phi}_q\sum_{k=1}^{n-1}\boldsymbol{\mu}^{n-k-1}\mathbf{Q_B}^{(k)} - \boldsymbol{\Phi}_q^*\sum_{k=n}^{N}\boldsymbol{\mu}^{k+1-n}\mathbf{Q_B}^{*(k)}, \tag{21}$$

$$-\mathbf{F}_L^{(n)} = \boldsymbol{\Phi}_F\boldsymbol{\mu}^{n-1}\mathbf{Q} + \boldsymbol{\Phi}_F^*\boldsymbol{\mu}^{N+1-n}\mathbf{Q}^* + \boldsymbol{\Phi}_F\sum_{k=1}^{n-1}\boldsymbol{\mu}^{n-k-1}\mathbf{Q_B}^{(k)} - \boldsymbol{\Phi}_F^*\sum_{k=n}^{N}\boldsymbol{\mu}^{k+1-n}\mathbf{Q_B}^{*(k)}, \tag{22}$$

with $\mathbf{Q} \equiv \mathbf{Q}^{(1)}$ and $\mathbf{Q}^* \equiv \mathbf{Q}^{*(N+1)}$. The unknown, frequency-dependent amplitude vectors $\mathbf{Q}$ and $\mathbf{Q}^*$ can be determined by imposing boundary conditions, and by considering externally applied loads, which show up in $\mathbf{Q}_B^{(k)}$, $\mathbf{Q}_B^{*(k)}$.

When some defect is introduced in a periodic structure, it can be envisioned as being made of multiple waveguides (WGs), as suggested by Fig. 1. In this context, the dynamic behaviors of distinct unit cells differ, such that Eqs. (21) and (22) need to be applied with care, taking into account the wavemodes of the unit cell of each particular WG (Santos, 2022). Of course, compatibility and equilibrium between WGs which are neighbors must be enforced to model the complete system. For the sake of simplicity, we consider each defective unit cell corresponds to a single WG.

NUMERICAL SIMULATIONS

Results presented in the sequence are related to a zig-zag beam-type quasi-periodic structure. The location of defects vary, being distinguished by the indexing number of defective unit cells along the lattice. The material is assumed to have linear isotropic behavior, with $E = 3$ GPa, $\nu = 0.3$ and $\rho = 1200\ \mathrm{kg/m^3}$. One recognizes that the investigations we consider next might be significantly influenced by the consideration of damping. Despite this realization, damping is not taken into account by us. The geometry of regular and defective unit cells, as well as finite element (FE) meshes used for assessing mass and stiffness properties, are shown in Fig. 3.

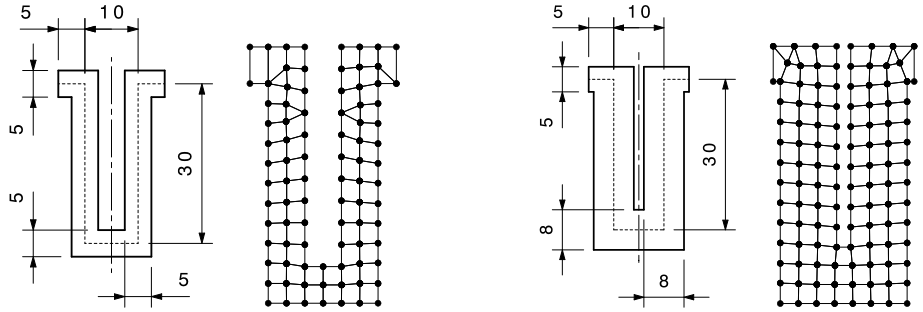

Figure 3 – Geometry and FE mesh of regular (left) and defective (right) unit cells. Dimensions are in mm.

The FE modeling has been performed with plate elements, based on Reissner-Mindlin theory, employing quadrilateral and triangular elements with six DOFs per node. A thickness of 1 mm was assumed for both regular and defective cells. The total number of unit cells of the quasi-periodic structure was taken as $N = 10$. In addition, the complete wave basis was admitted for all WGs of the zig-zag beam, corresponding to 12 pairs of wavemodes.

Transmissibilities were calculated by imposing a 1 mm z-displacement at the left extremity of the various analyzed quasi-periodic lattices and observing the corresponding motion at their right end, as depicted in Fig. 4, for a particular condition in which the defects are located at cells 7 and 10. So, Fig. 5 shows some of these results, related to a quasi-

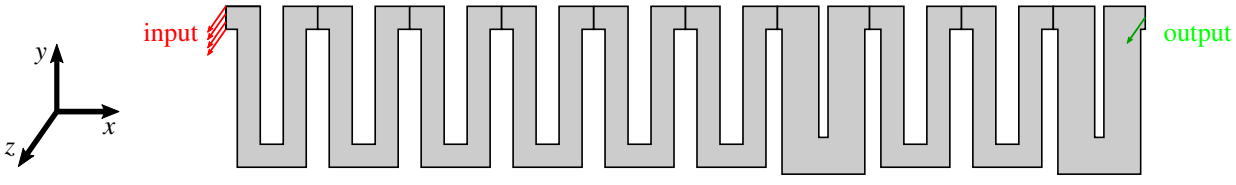

Figure 4 – Input and output locations assumed in this work to compute transmissibilities.

periodic structure with only regular unit cells (blue line) and quasi-periodic structures with imperfections at cell 4 (red line) and at cells 4 and 8 (black dotted line). In addition, Fig. 5 also displays in shaded area the bandgap calculated to an infinite periodic structure, made with regular unit cells, comprising the frequency range from 200 to 580 Hz.

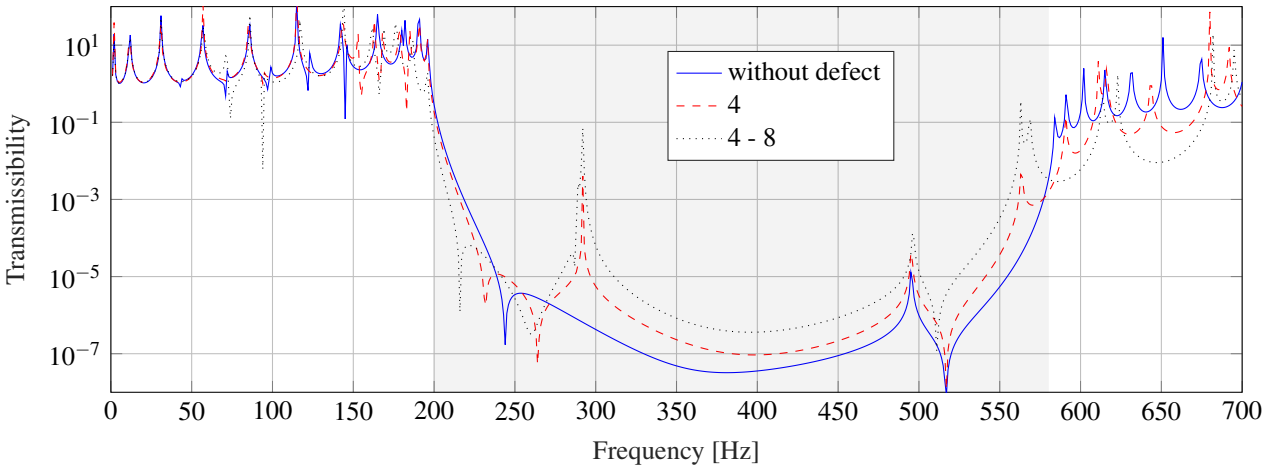

Figure 5 – Transmissibility computed for quasi-periodic structures.

From Fig. 5, we notice that localized modes can be seen after the inclusion of one or two defective unit cells, which correspond to the various sharp peaks occurring within the bandgap frequency range. For the lattice without defective unit cells, only one localized mode can be observed, corresponding to the frequency of 495 Hz and being related to the motion of the lattice confined to its left extremity, i.e., where the energy is put into the system. While this may appear unexpected, one should realize that boundaries also break the periodicity of an otherwise repetitive arrangement of unit cells. Due to the inclusion of defective unit cells, three additional localized modes appear, corresponding to the frequencies 292, 563, and 569 Hz. For these, motion and energy get concentrated at the defect locations – which also may include the left boundary –, comprising out-of-plane bending modes. A summary of these frequencies is provided in Table 1.

Table 1 – Summary of the frequencies corresponding to the localized modes which can be identified from Fig. 5.

Defect locations	Frequency [Hz]
without defect	495
4	292, 495, 563
4 - 8	292, 495, 563, 569

One also realizes from Fig. 5 that all the transmissibilities are very similar, up to 100 Hz. On the other hand, noticeable differences between the curves can be seen close to the beginning of the bandgap. The similarities between the transmissibilities seem to decrease strongly after the end of the bandgap frequency range. In addition, albeit the dynamic behavior of the zig-zag beam-type structure gets changed above 100 Hz, we draw attention to the fact that the bandgap frequency range is mostly unaffected. For a better understanding of the zig-zag beams' dynamics, harmonic deformed shapes are shown in Fig. 6 for the various localized modes' whose frequencies were seen in Fig. 5 (cf. Table 1). From these simulations, it is possible to notice that the inclusion of two defects in the lattice makes some localized modes show additional deformation at the other defective unit cell, which allows for generating an extra localized mode (at 569 Hz). Moreover, one recognizes that the inclusion of defects does not seem to change the deformed patterns of the localized modes corresponding to the frequency of 495 Hz, i.e., energy maintains concentrated at the left boundary of the quasi-periodic structure in all of them.

From the results discussed above, we may also investigate if the separation distance between two defective unit cells contributes to the formation of additional localized modes. In addition, one may also be interested in investigating if the bandgap frequency range of the modified structures differs from the one estimated through the Bloch-Floquet theorem for the infinite periodic structure composed of regular unit cells. To examine this, transmissibility results have also been obtained, employing the same conditions established earlier, being them shown in Fig. 7 (a summary of the frequencies corresponding to the localized modes is given in Table 2).

Similarly to results seen previously, Fig. 7 depicts that the transmissibilities almost do not change up to 100 Hz. In addition, one can also see that the differences between the curves become apparent near the beginning of the bandgap, whereas they are strongly accentuated after 580 Hz. It can also be noted that the forbidden zone appears to not be changed

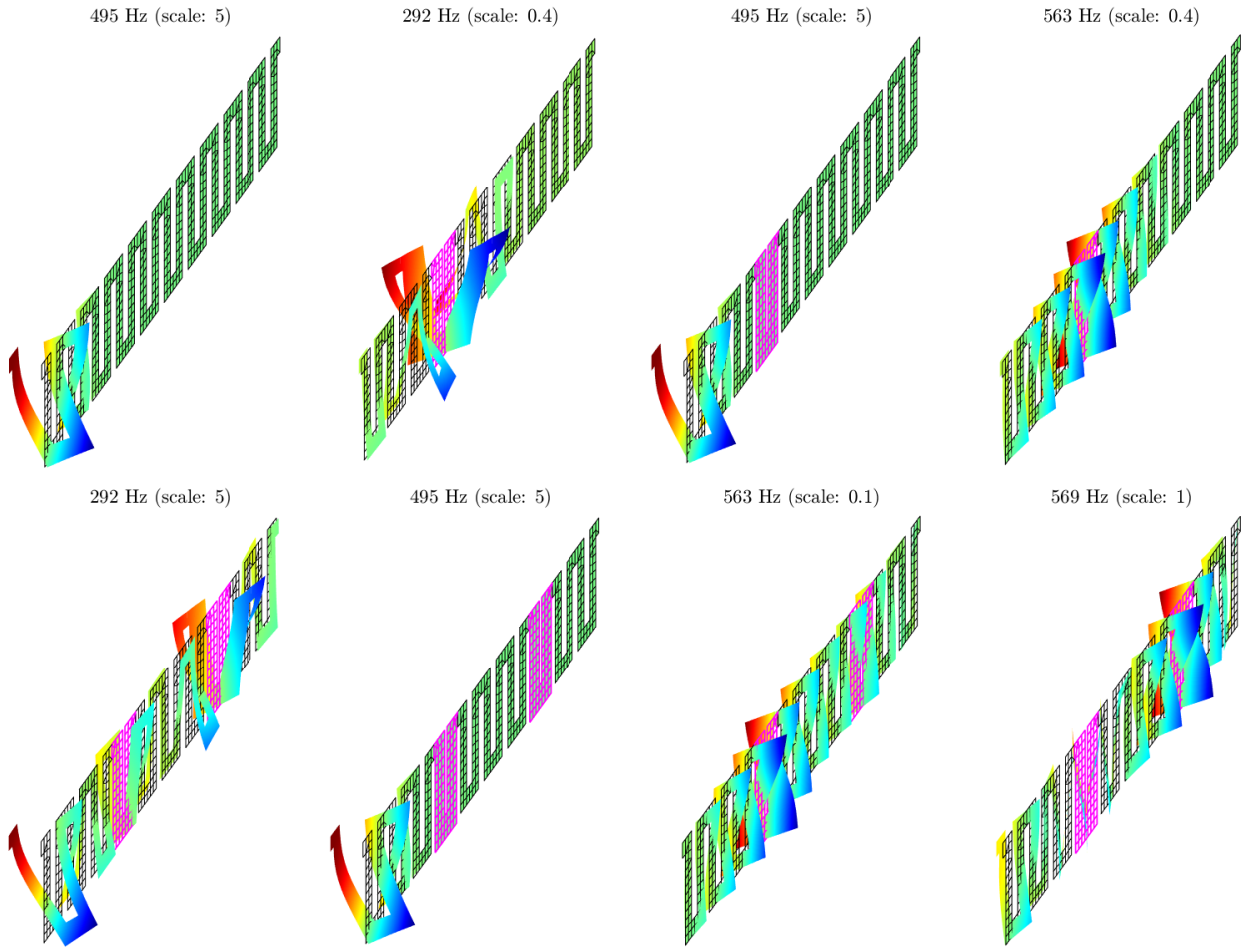

Figure 6 – Deformed patterns computed for frequencies occurring within the bandgap frequency range portrayed in Fig. 5. The undeformed mesh is also shown in black lines, being defective unit cells colored in magenta.

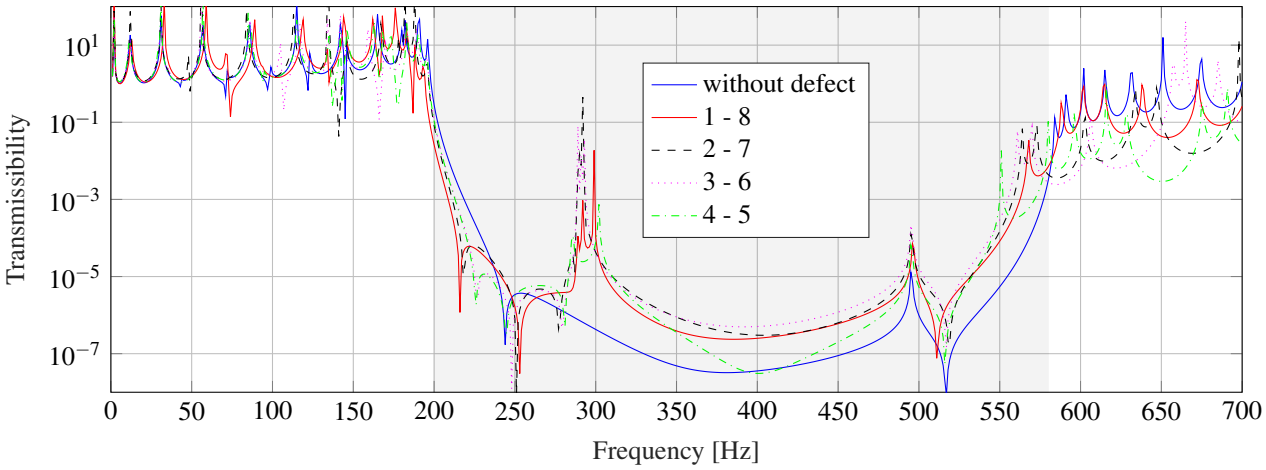

Figure 7 – Transmissibility calculated to investigate how the separation distance between defects affects the dynamics of the zig-zag beam system.

after the defects were added. Furthermore, Fig. 7 shows exactly the same number of peaks occurring within the bandgap frequency range, related to localized modes, for the configurations in which the defects are located at cells 1 - 8, 2 - 7, and 3 - 6 (cf. Table 2). On the other hand, when the defective cells are placed as near as possible, the corresponding transmissibility exhibit one less resonance frequency between 200 and 580 Hz. This absence of a localized mode is explained because both defective cells resonate together without creating an additional peak in the transmissibility that could appear if the defects were positioned at some separation distance. Figure 8 illustrates a couple of bending modes that resonate at frequencies 302 Hz and 551 Hz, being possible to confirm the previous statement.

Table 2 – Summary of the frequencies corresponding to the localized modes which can be identified from Fig. 7.

Defect locations	Frequency [Hz]
without defect	495
1 - 8	289, 292, 299, 495, 569
2 - 7	289, 292, 495, 564, 573
3 - 6	289, 292, 495, 561, 570
4 - 5	286, 302, 495, 551

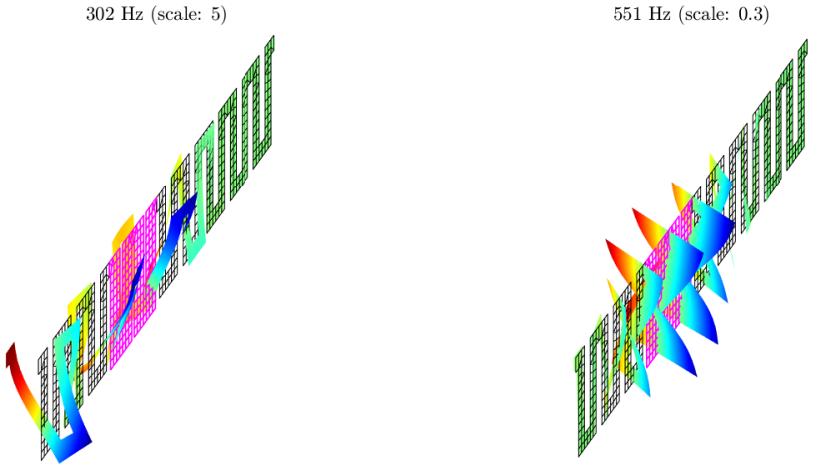

Figure 8 – Deformed patterns computed to illustrate a couple of bending localized modes in which both defective unit cells resonate simultaneously (at the same frequency) due to their positions in the quasi-periodic structure.

It should also be interesting to understand how the placement of a pair of defective unit cells along the zig-zag beam quasi-periodic system, separated by a constant distance of two defects, for example, affects its dynamic behavior. Assuming conditions reported earlier for input and output locations (cf. Fig. 4), Fig. 9 shows transmissibility curves calculated for various analyzed configurations. Once again, one notices there exists a trend of all transmissibilities being similar up to 100 Hz so that the bandgap frequency range is a watershed in the dynamic behavior of the zig-zag beam-type quasi-periodic structure. In addition, the bang gap calculated for an infinite periodic structure, made with regular unit cells, seems to match the frequency range that the quasi-periodic structures exhibit a low level of response. Furthermore, when the defects are located at cells 2 - 5, 3 - 6, 4 - 7, 5 - 8, and 6 - 9, the zig-zag beam-type quasi-periodic structure exhibit five localized modes (cf. Table 3). However, when one of the defects pertains to the ends of the structure, the computed transmissibilities reveal one less resonance within the bandgap frequency range.

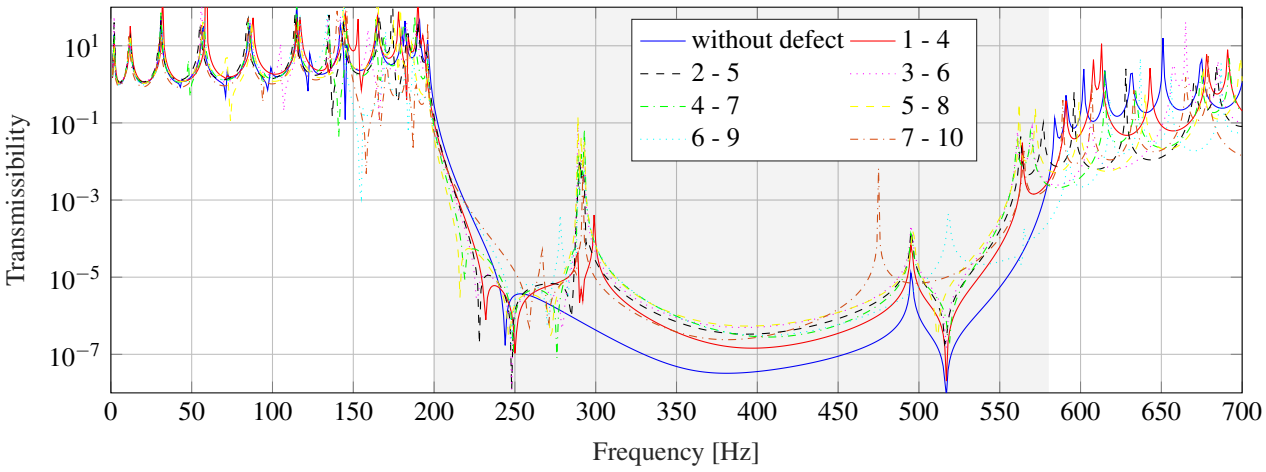

Figure 9 – Transmissibilities computed to investigate how the location of defects, for a constant gap between them, affects the dynamics of the zig-zag beam system.

Table 3 – Summary of the frequencies corresponding to the localized modes which can be identified from Fig. 9.

Defect locations	Frequency [Hz]
without defect	495
1 - 4	289, 299, 495, 564
2 - 5	290, 292, 495, 564, 577
3 - 6	289, 293, 495, 561, 570
4 - 7	289, 293, 495, 561, 569
5 - 8	289, 293, 496, 562, 572
6 - 9	278, 291, 293, 518, 565
7 - 10	267, 292, 475, 565

The absence of one localized mode within the bandgap frequency range when the defects are placed at cells 1 - 4 and 7 - 10 may be justified case-by-case. First, for the configuration that the defects are placed at cells 1 - 4, one of the localized modes arising from the defect inclusion occurs exactly at the left boundary so that the effect of generating localized modes from the defect inclusion is forfeit – since one also expected at least one localized mode at the left boundary (cf. Fig. 6, for example). This behavior is depicted in Fig. 10 for two localized modes, where it is possible to see that energy gets confined in the system's left end, which coincides with the placement of the defects.

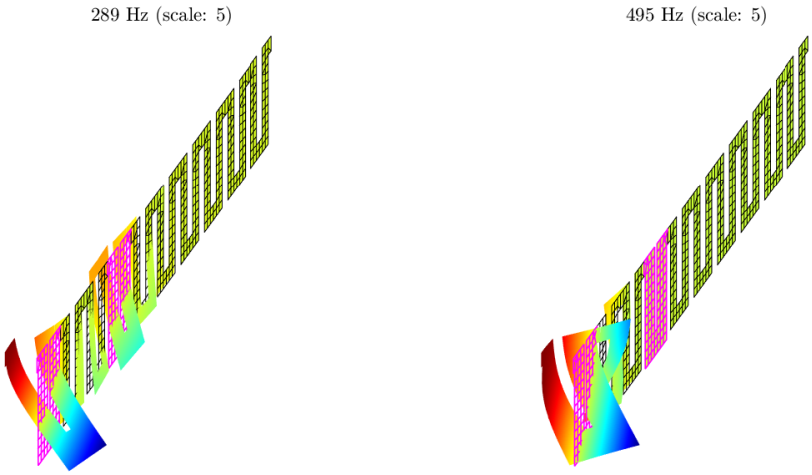

Figure 10 – Deformed patterns computed to illustrate localized modes ensuing at the left end of the zig-zag beam structure, where defective cells were placed.

On the other hand, when the defects are located at cells 7 - 10, i.e., as far as possible from the excitation location, one of the defective cells (10) can not contribute to the formation of a localized mode in the system's first bandgap frequency range. This result occurs because waves are forbidden to propagate within the bandgap frequency range, i.e., they are highly evanescent. So energy cannot propagate a long distance to reach the defective cell located at the right end of the zig-zag beam quasi-periodic structure. Deformed patterns computed for the frequencies occurring within the bandgap when the defects are located at cells 7 - 10 are shown in Fig. 11 to clarify the latter comments.

CONCLUDING REMARKS

In this article, the dynamic behavior of a zig-zag beam-type quasi-periodic structure is assessed to evaluate how the positioning of a couple of defective unit cells influences its localized modes in terms of frequencies and deformed patterns. Simulations were carried out using the WFEM while taking into account connectivity conditions that must be fulfilled by neighboring WGs. Numerical results have shown that the dynamic behavior of the zig-zag structure is mostly unaffected up to 100 Hz in the presence of defective cells. On the other hand, discrepancies between the transmissibilities computed were evidenced close to the beginning of the bandgap, i.e., between 100 and 200 Hz. These differences were greatly accentuated after the end of the bandgag frequency range at 580 Hz. Despite the fact that the dynamic behavior of the zig-zag beam-type quasi-periodic structure is changed above 100 Hz when defects are embedded in its lattice in various locations, it was possible to verify by inspection of transmissibilities that the bandgap frequency range of the analyzed configurations seems to not be changed compared to the one computed for an infinite regular periodic structure through the Bloch-Floquet theorem. In addition, we show that when the separation distance between defects is zero, i.e., defective cells are neighbors, the computed transmissibility exhibits one less localized mode because the defects are not

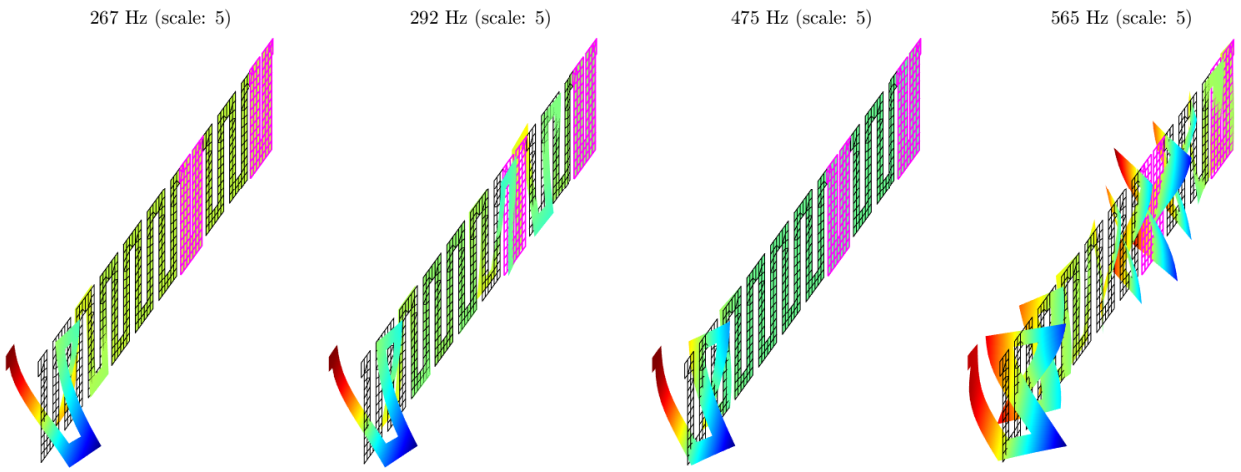

Figure 11 – Deformed patterns computed for frequencies occurring within the bandgap frequency range for the condition in which the defects are located at cells 7 - 10, corresponding to the transmissibility depicted in Fig. 9.

able to generate localized modes in distinct resonance frequencies. In this setting, the defective cells resonate together, being necessary some distance between them for the localization phenomena to be exploited. In addition, simulations performed by varying the location of defects, maintaining a constant distance between them, have shown that a large number of localized modes can be obtained if one of the defective cells is not placed at the left boundary of the zig-zag beam-type structure. These results suggest that the dynamic behavior of quasi-periodic structures can be enhanced for some particular engineering applications in which it might be used, such as energy harvesting, for example, when a couple of defects are used unlike one. Of course, the position of the defects can favor (or not) the formation of localized modes in the quasi-periodic systems, and it must be carefully considered.

ACKNOWLEDGMENTS

V.M.S. Santos acknowledges his doctorate scholarship by the Brazilian Coordination for the Improvement of Higher Education Personnel (CAPES) and also his master scholarship by the Brazilian National Council for Scientific and Technological Development (CNPq). Both authors are grateful to the São Paulo Research Foundation (FAPESP) for its support to the thematic grant #18/15894-0, related to the "Periodic structure design and optimization for enhanced vibroacoustic performance: ENVIBRO" research project.

REFERENCES

Anderson, P.W., 1958, "Absence of Diffusion in Certain Random Lattices", Physical Review, Vol. 109, No. 5, pp. 1492–1505.

Assouar, M.B., Senesi, M., Oudich, M., Ruzzene, M. and Hou, Z., 2012, "Broadband plate-type acoustic metamaterial for low-frequency sound attenuation", Applied Physics Letters, Vol. 101, No. 17, p. 173505.

Bendiksen, O., 2000, "Localization phenomena in structural dynamics", Chaos, Solitons & Fractals, Vol. 11, No. 10, pp. 1621–1660.

Brillouin, L., 1955, "Wave Propagation in Periodic Structures", Dover.

Cunha, L., 2017, "Robust bandgaps for vibration control in periodic structures", Ph.D. thesis, EDUFU - Editora da Universidade Federal de Uberlandia.

Duhamel, D., Mace, B. and Brennan, M., 2006, "Finite element analysis of the vibrations of waveguides and periodic structures", Journal of Sound and Vibration, Vol. 294, No. 1-2, pp. 205–220.

Hoang, T., Duhamel, D. and Forêt, G., 2018, "Wave finite element method for vibration of periodic structures subjected to external loads", 6th European Conference on Computational Mechanics (ECCM 6), Glasgow, United Kingdom, pp. 1–11.

Hodges, C., 1982, "Confinement of vibration by structural irregularity", Journal of Sound and Vibration, Vol. 82, No. 3, pp. 411–424.

Jo, S.H., Yoon, H., Shin, Y.C., Choi, W., Park, C.S., Kim, M. and Youn, B.D., 2020, "Designing a phononic crystal with a defect for energy localization and harvesting: Supercell size and defect location", International Journal of Mechanical Sciences, Vol. 179, p. 105670.

Luongo, A., 1992, "Mode localization by structural imperfections in one-dimensional continuous systems", Journal of Sound and Vibration, Vol. 155, No. 2, pp. 249–271.

Mace, B.R., Duhamel, D., Brennan, M.J. and Hinke, L., 2005, "Finite element prediction of wave motion in structural waveguides", The Journal of the Acoustical Society of America, Vol. 117, No. 5, pp. 2835–2843.

Mencik, J.M., 2014, "New advances in the forced response computation of periodic structures using the wave finite element (WFE) method", Computational Mechanics, Vol. 54, No. 3, pp. 789–801.

Mencik, J.M. and Duhamel, D., 2015, "A wave-based model reduction technique for the description of the dynamic behavior of periodic structures involving arbitrary-shaped substructures and large-sized finite element models", Finite Elements in Analysis and Design, Vol. 101, pp. 1–14.

Mencik, J.M. and Ichchou, M., 2005, "Multi-mode propagation and diffusion in structures through finite elements", European Journal of Mechanics - A/Solids, Vol. 24, No. 5, pp. 877–898.

Mizukami, K., Funaba, K. and Ogi, K., 2021, "Design and three-dimensional printing of carbon-fiber-composite elastic metamaterials with inertial amplification mechanisms", Journal of Sound and Vibration, Vol. 513, p. 116412.

Pal, R.K. and Ruzzene, M., 2017, "Edge waves in plates with resonators: an elastic analogue of the quantum valley Hall effect", New Journal of Physics, Vol. 19, No. 2, p. 025001.

Renno, J.M. and Mace, B.R., 2010, "On the forced response of waveguides using the wave and finite element method", Journal of Sound and Vibration, Vol. 329, No. 26, pp. 5474–5488.

Santos, V., 2022, "Numerical investigation of wave propagation in beams coupled to metastructures combining spectral and wave-finite element methods", Master's thesis, Aeronautics Institute of Technology.

Waki, Y., Mace, B. and Brennan, M., 2009a, "Free and forced vibrations of a tyre using a wave/finite element approach", Journal of Sound and Vibration, Vol. 323, No. 3-5, pp. 737–756.

Waki, Y., Mace, B. and Brennan, M., 2009b, "Numerical issues concerning the wave and finite element method for free and forced vibrations of waveguides", Journal of Sound and Vibration, Vol. 327, No. 1-2, pp. 92–108.

Zhong, W. and Williams, F., 1995, "On the direct solution of wave propagation for repetitive structures", Journal of Sound and Vibration, Vol. 181, No. 3, pp. 485–501.

Zhu, H. and Semperlotti, F., 2013, "Metamaterial based embedded acoustic filters for structural applications", AIP Advances, Vol. 3, No. 9, p. 092121.

RESPONSIBILITY NOTICE

The authors are the only responsible for the printed material included in this paper.